Quantum transport through a graphene nanoribbon–superconductor junction

2009 J. Phys.: Condens. Matter 21 344204

(http://iopscience.iop.org/0953-8984/21/34/344204)

IOP Publishing Journal of Physics: Condensed Matter

J. Phys.: Condens. Matter **21** (2009) 344204 (9pp) doi:10.1088/0953-8984/21/34/344204

Quantum transport through a graphene nanoribbon–superconductor junction

Qing-feng Sun[1] **and X C Xie**[1,2]

[1] Beijing National Lab for Condensed Matter Physics and Institute of Physics, Chinese Academy of Sciences, Beijing 100190, People's Republic of China
[2] Department of Physics, Oklahoma State University, Stillwater, OK 74078, USA

E-mail: sunqf@aphy.iphy.ac.cn

Received 13 April 2009
Published 27 July 2009
Online at stacks.iop.org/JPhysCM/21/344204

Abstract

We study the electron transport through a graphene nanoribbon–superconductor junction. Both zigzag and armchair edge graphene nanoribbons are considered, and the effects of the magnetic field and disorder on the transport property are investigated. By using the tight-binding model and the non-equilibrium Green's function method, the expressions of the current, conductance, normal tunneling coefficient and Andreev reflection coefficient are obtained. For a clean system and at zero magnetic field, the linear conductance increases approximately in a linear fashion with the on-site energy. In the presence of a magnetic field and a moderate disorder, the linear conductance exhibits plateau structures for both armchair and zigzag edges. The plateau values increase with the width of the graphene ribbon. With a wide sample width, a saturated plateau value of $|\nu|e^2/h$ emerges at the filling factor ν. For a small filling factor, the conductance can reach the saturated value at a small width, but for a high filling factor it requires to have a quite wide sample width to reach the saturated value. In particular, the Andreev reflection coefficient is always at 0.5 after reaching the saturated value, independent of any system parameters. In addition, we also consider the finite bias case, in which the Andreev reflection coefficient and normal tunneling coefficient are studied.

(Some figures in this article are in colour only in the electronic version)

1. Introduction

The recent experimental realization of graphene [1, 2], a single layer of carbon atoms arranged in a honeycomb lattice, has generated a great deal of attention in the condensed matter community [3, 4]. Graphene has an unique band structure with a linear dispersion relation of the low-lying excitations, which leads to many peculiar properties [3, 4], such as its quasi-particles obeying the Dirac-like equation and having relativistic-like behavior with zero rest mass and the Hall plateaus having the half-integer values $g(n + 1/2)e^2/h$ with the degeneracy $g = 4$. For the neutral graphene, its Fermi level passes through the Dirac points, the six corners of the hexagonal first Brillouin zone. By varying the gate voltage, the charge carriers of graphene can be easily tuned experimentally. Then the Fermi level can be above or below the Dirac points.

Very recently, some works have begun to investigate the transport behavior of the graphene–superconductor junctions [5–17]. While a metal coupled to a superconductor, the Andreev reflection occurs in the interface between the metal and superconductor [18], in which the interface reflects an electron incident from the normal metal side as a hole and a Cooper pair is created in the superconductor. For a bias below the superconductor gap, the Andreev reflection determines the conductance of the metal–superconductor junction since the normal tunneling cannot occur. In the usual metal–superconductor junction, the Andreev reflected hole retraces the path of the incident electron, so this Andreev reflection is also called Andreev retroreflection. But for the graphene–superconductor junction, Beenakker recently found that a new kind of reflection (specular Andreev reflection) occurs while the incident electron and reflected hole are at the conduction and valence bands, respectively [5]. Afterward, many papers have studied the graphene and superconductor hybrid system, including the graphene-based normal–superconductor (N–S) [5–7, 14], S–N–S [8–10], S–insulator–S [13], S–ferromagnet–S [11], etc. Several other effects due to the coupling of graphene and superconductor, such as the

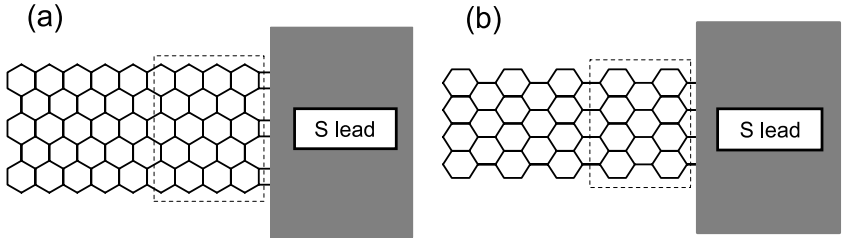

Figure 1. (a) and (b) are the schematic diagrams for the zigzag and armchair edge graphene nanoribbon–superconductor junctions, respectively.

Josephson effect [8, 9, 13] and multiple Andreev reflection processes [15], have been theoretically analyzed. On the experimental side, good contacts between the superconductor electrodes and graphene have been realized [19, 20] and the Josephson current through an S–graphene–S junction has been measured. A finite supercurrent was observed at zero charge density.

In this paper, we carry out a theoretical study of the transport characteristics of a graphene nanoribbon–superconductor junction. There are four new aspects beyond the previous studies: (i) we study the system consisting of a graphene nanoribbon with a finite width coupled to the superconductor electrode. The previous theoretical papers only consider the infinite-width graphene–superconductor junction or a graphene strip between two superconductor leads with the strip width much larger than the strip length. On the experimental side, the graphene nanoribbon has been successfully fabricated and the width of the nanoribbon can be of the order of ten or sub-ten nanometers [21]. (ii) In our model, the graphene nanoribbon is directly coupled to the superconductor electrode and the incident electrons from the graphene are allowed to enter into the superconductor electrode as the Cooper pairs. In the previous papers, those authors only considered a pair potential in the graphene induced by depositing of a superconductor electrode on top of the graphene sheet. (iii) We consider a perpendicular magnetic field applied to the graphene, as was done in a recent experiment [19]. On the superconductor side, the magnetic field vanishes due to the Meissner effect. (iv) The effect of disorder on the transport property is investigated since, in a real graphene sample, the disorder is always there to a certain degree. In fact, in the previous studies, the effects of disorder and magnetic field are thus far neglected.

By using the tight-binding model and the non-equilibrium Green function method, the current and Andreev reflection coefficient are obtained. Both zigzag edge and armchair edge graphene nanoribbons are considered. For the zigzag edge and at a zero magnetic field, the linear conductance exhibits step structures for the narrow graphene ribbon. With a magnetic field, the conductance depends strongly on the system parameters. In the presence of disorder, the linear conductance shows plateaus at a high magnetic field. On the other hand, for the armchair edge, a zero conductance region emerges because of the existence of an energy gap in the graphene nanoribbon. This zero conductance is robust against disorder. In addition, we also consider a finite bias case, in which the Andreev reflection coefficient and normal tunneling coefficient are investigated.

The rest of this paper is organized as follows. In section 2, the model for graphene nanoribbon–superconductor junction is presented and the formalisms for calculating the current and the Andreev reflection coefficient are derived. In sections 3 and 4, we study the linear conductance and the transport with a finite bias, respectively. Finally, a brief summary is presented in section 5.

2. Model and formalism

We consider the system consisting of a graphene nanoribbon coupled to a superconductor lead (as shown in figure 1) with the Hamiltonian

$$H = H_{\mathrm{G}} + H_{\mathrm{S}} + H_{\mathrm{C}}, \tag{1}$$

where H_{G}, H_{S} and H_{C} are the Hamiltonians of the graphene region, superconductor lead and coupling of the graphene and superconductor lead, respectively. For a semi-infinite graphene nanoribbon, H_{G} in the tight-binding representation is of the form [22, 23]

$$H_{\mathrm{G}} = \sum_{i,\sigma} \epsilon_i a_{i\sigma}^{\dagger} a_{i\sigma} - \sum_{\langle ij\rangle,\sigma} t \mathrm{e}^{\mathrm{i}\phi_{ij}} a_{i\sigma}^{\dagger} a_{j\sigma}, \tag{2}$$

where $a_{i\sigma}$ and $a_{i\sigma}^{\dagger}$ are the annihilation and creation operators at the discrete site i, and ϵ_i is the on-site energy which can be controlled by the gate voltage in an experiment. Two kinds of edges, zigzag and armchair, are considered (see figures 1(a) and (b)). The graphene ribbon is divided into two regions. The left side of the semi-infinite region is without disorder and $\epsilon_i = E_{\mathrm{L}}$ there. The disorder exists only in the center region of the graphene–nanoribbon (see the box with the dotted line in figure 1). Here we consider the on-site disorder caused by the nonmagnetic impurities or by the random potential difference of the substrate. Due to the disorder, the on-site energy $\epsilon_i = E_{\mathrm{L}} + w_i$, where w_i is the on-site disorder energy and w_i is uniformly distributed in the range $[-W/2, W/2]$ with W being the disorder strength. The size of the disordered region is described by the width N and length L. In figures 1(a) and (b), $N = 3$, $L = 4$ and $N = 4$, $L = 2$, respectively. The second term in equation (2) is the nearest-neighbor hopping. When the graphene ribbon is under a uniform perpendicular magnetic field B, a phase ϕ_{ij} is added in the hopping elements, and

$\phi_{ij} = \int_i^j \vec{A}\cdot \mathrm{d}\vec{l}/\phi_0$ with the vector potential $\vec{A} = (-By, 0, 0)$ and $\phi_0 = \hbar/e$.

Experimentally, it is possible to have the superconductor electrode in good contact with the graphene [19]. The electrons from the graphene can easily enter into the superconductor electrode as the Cooper pairs or vice versa. So we consider that the graphene nanoribbon is directly coupled to the superconductor electrode. The superconductor electrode is described by a continuum model and it does not have the honeycomb structure of the graphene. Then the Hamiltonian H_S is

$$H_S = \sum_{\mathbf{k},\sigma} \epsilon_{\mathbf{k}} b^\dagger_{\mathbf{k}\sigma} b_{\mathbf{k}\sigma} + \sum_{\mathbf{k}} (\Delta b^\dagger_{\mathbf{k}\uparrow} b^\dagger_{-\mathbf{k}\downarrow} + \Delta b_{-\mathbf{k}\downarrow} b_{\mathbf{k}\uparrow}), \quad (3)$$

where $b_{\mathbf{k}\sigma}$ and $b^\dagger_{\mathbf{k}\sigma}$ are the annihilation and creation operators in the superconductor lead with the momentum $\mathbf{k} = (k_x, k_y)$. Here we consider the s-wave superconductor and Δ is the superconductor gap. The superconductor region is without the magnetic field due to the Meissner effect or that the magnetic field is only added in the graphene region. The Hamiltonian H_C of the coupling between the superconductor lead and the graphene nanoribbon is

$$H_C = \sum_{i,\sigma} t_c a^\dagger_{i\sigma} b_\sigma(y_i) + \text{h.c.} \quad (4)$$

Here only the surface carbon atoms couple to the superconductor lead and y_i is the vertical position of the carbon atom i. $b_\sigma(y)$ is the annihilation operators at the position $(0, y)$ of real space and

$$b_\sigma(y) = \sum_{k_x,k_y} \mathrm{e}^{\mathrm{i}k_y y} b_{\mathbf{k}\sigma}. \quad (5)$$

The current flowing through the graphene nanoribbon–superconductor junction can be calculated from the evolution of the total number operator for electrons in the left graphene–nanoribbon lead [24]:

$$I = -e\left\langle \frac{\mathrm{d}}{\mathrm{d}t} \sum_{i\in L,\sigma} a^\dagger_{i\sigma} a_{i\sigma} \right\rangle = \frac{e}{\hbar} \sum_{i\in L, j\in C} \int \frac{\mathrm{d}\omega}{2\pi} \times \{t_{ij} G^<_{ji,11} - t_{ij} G^<_{ij,22} - t_{ji} G^<_{ij,11} + t_{ji} G^<_{ji,22}\}, \quad (6)$$

where $t_{ij} = t\mathrm{e}^{\mathrm{i}\phi_{ij}}$. Here $i \in L$ and $j \in C$ represent that the site index i and j are in the left graphene lead and center region. $\mathbf{G}^<_{ij}(\omega)$ is the matrix Green function in Nambu representation, and it is the Fourier transformation of $\mathbf{G}^<_{ij}(t)$:

$$\mathbf{G}^<_{ij}(t) = \mathrm{i}\begin{pmatrix} \langle a^\dagger_{j\uparrow}(0) a_{i\uparrow}(t)\rangle & \langle a_{j\downarrow}(0) a_{i\uparrow}(t)\rangle \\ \langle a^\dagger_{j\uparrow}(0) a^\dagger_{i\downarrow}(t)\rangle & \langle a_{j\downarrow}(0) a^\dagger_{i\downarrow}(t)\rangle \end{pmatrix}. \quad (7)$$

By using the Dyson equation, the current expression in equation (6) can be rewritten as

$$I = \frac{e}{h}\int \mathrm{d}\omega\, \mathrm{Tr}\begin{pmatrix} 1 & 0 \\ 0 & -1 \end{pmatrix} \bigotimes \mathbf{I}_{Nc} \{(\mathbf{\Sigma}^a_L - \mathbf{\Sigma}^r_L)\mathbf{G}^< + \mathbf{\Sigma}^<_L(\mathbf{G}^r - \mathbf{G}^a)\}. \quad (8)$$

Here $\mathbf{G}^{r,a,<}(\omega)$ are the $2Nc \times 2Nc$ matrix Green's functions in the center region with Nc being the number of sites in the center region. The retarded and advanced Green's functions $\mathbf{G}^{r,a}$ are defined in the standard way [25]. $\mathbf{I}_{Nc}$ is the $Nc \times Nc$ unit matrix. $\mathbf{\Sigma}^{r,a,<}_L(\omega)$ are the retarded, advanced and lesser self-energies of coupling to the left graphene lead, and they are

$$\mathbf{\Sigma}^r_{L,ij} = \sum_{n\in L, m\in L} \begin{pmatrix} t_{in}\mathbf{g}^r_{nm,11} t_{mj} & 0 \\ 0 & t^*_{in}\mathbf{g}^r_{nm,22} t^*_{mj} \end{pmatrix} \quad (9)$$

$$\mathbf{\Sigma}^a_L = \mathbf{\Sigma}^{r\dagger}_L \quad (10)$$

$$\mathbf{\Sigma}^<_L = \begin{pmatrix} \mathrm{i} f_\uparrow(\omega)\mathbf{\Gamma}_{L\uparrow}(\omega) & 0 \\ 0 & \mathrm{i} f_\downarrow(\omega)\mathbf{\Gamma}_{L\downarrow}(\omega) \end{pmatrix}, \quad (11)$$

where $f_\uparrow(\omega) = f(\omega - eV)$ and $f_\downarrow(\omega) = f(\omega + eV)$, with V being the bias voltage and $f(\omega)$ being the Fermi distribution function, and $\mathbf{\Gamma}_{L\uparrow}(\omega) \equiv \mathrm{i}(\mathbf{\Sigma}^r_L - \mathbf{\Sigma}^a_L)_{11}$ and $\mathbf{\Gamma}_{L\downarrow}(\omega) \equiv \mathrm{i}(\mathbf{\Sigma}^r_L - \mathbf{\Sigma}^a_L)_{22}$. $\mathbf{g}^r_{nm}(\omega)$ in equation (9) is the surface Green's function of the semi-infinite graphene nanoribbon, which can be numerically calculated [26]. With the aid of the self-energy functions in equations (9)–(11), the current I is finally reduced to

$$I = I_\uparrow + I_\downarrow, \quad (12)$$

$$I_\uparrow = \frac{\mathrm{i}e}{h}\int \mathrm{d}\omega\, \mathrm{Tr}\,\mathbf{\Gamma}_{L\uparrow}\{\mathbf{G}^< + f_\uparrow(\mathbf{G}^r - \mathbf{G}^a)\}_{11}, \quad (13)$$

$$I_\downarrow = -\frac{\mathrm{i}e}{h}\int \mathrm{d}\omega\, \mathrm{Tr}\,\mathbf{\Gamma}_{L\downarrow}\{\mathbf{G}^< + f_\downarrow(\mathbf{G}^r - \mathbf{G}^a)\}_{22}. \quad (14)$$

As shown in the appendix, the self-energies $\mathbf{\Sigma}^{r,a,<}_R$ of coupling to the superconductor lead can be obtained by $\mathbf{\Sigma}^r_R = -(\mathrm{i}/2)\mathbf{\Gamma}_R$, $\mathbf{\Sigma}^a_R = (\mathrm{i}/2)\mathbf{\Gamma}_R$ and $\mathbf{\Sigma}^<_R = \mathrm{i}f(\omega)\mathbf{\Gamma}_R$. Then by using the Keldysh equation $\mathbf{G}^< = \mathbf{G}^r\mathbf{\Sigma}^<\mathbf{G}^a$, $\mathbf{G}^r - \mathbf{G}^a = \mathbf{G}^r(\mathbf{\Sigma}^r - \mathbf{\Sigma}^a)\mathbf{G}^a$ and the self-energies $\mathbf{\Sigma}^{r,a,<} = \mathbf{\Sigma}^{r,a,<}_L + \mathbf{\Sigma}^{r,a,<}_R$, the currents $I_\uparrow$ and $I_\downarrow$ can be rewritten as

$$I_\uparrow = \frac{e}{h}\int \mathrm{d}\omega\, \mathrm{Tr}\{\mathbf{\Gamma}_{L\uparrow}[\mathbf{G}^r\mathbf{\Gamma}_R\mathbf{G}^a]_{11}(f_\uparrow - f) + \mathbf{\Gamma}_{L\uparrow}\mathbf{G}^r_{12}\mathbf{\Gamma}_{L\downarrow}\mathbf{G}^a_{21}(f_\uparrow - f_\downarrow)\}, \quad (15)$$

$$I_\downarrow = -\frac{e}{h}\int \mathrm{d}\omega\, \mathrm{Tr}\{\mathbf{\Gamma}_{L\downarrow}[\mathbf{G}^r\mathbf{\Gamma}_R\mathbf{G}^a]_{22}(f_\downarrow - f) + \mathbf{\Gamma}_{L\downarrow}\mathbf{G}^r_{21}\mathbf{\Gamma}_{L\uparrow}\mathbf{G}^a_{12}(f_\downarrow - f_\uparrow)\}. \quad (16)$$

Here $\mathrm{Tr}\{\mathbf{\Gamma}_{L\uparrow}[\mathbf{G}^r\mathbf{\Gamma}_R\mathbf{G}^a]_{11}\} \equiv T_\uparrow(\omega)$ and $\mathrm{Tr}\{\mathbf{\Gamma}_{L\downarrow}[\mathbf{G}^r\mathbf{\Gamma}_R\mathbf{G}^a]_{22}\} \equiv T_\downarrow(\omega)$ are the normal tunneling coefficients for the incident spin-up electron and spin-down hole with the energy ω, and $\mathrm{Tr}\{\mathbf{\Gamma}_{L\uparrow}\mathbf{G}^r_{12}\mathbf{\Gamma}_{L\downarrow}\mathbf{G}^a_{21}\} \equiv T_{A\uparrow}(\omega)$ and $\mathrm{Tr}\{\mathbf{\Gamma}_{L\downarrow}\mathbf{G}^r_{21}\mathbf{\Gamma}_{L\uparrow}\mathbf{G}^a_{12}\} \equiv T_{A\downarrow}(\omega)$ are the Andreev reflection coefficients. Since the Pauli matrices $\hat{\sigma}_{x,y,z}$ commute with the Hamiltonian H, the normal transmission coefficients $T_\uparrow(\omega) = T_\downarrow(-\omega) \equiv T(\omega)$ and the Andreev reflection coefficients $T_{A\uparrow}(\omega) = T_{A\downarrow}(-\omega) \equiv T_A(\omega)$.

In the following, we need to calculate the Green's functions $\mathbf{G}^r$ and $\mathbf{G}^a$ of the center region. Since the self-energy $\mathbf{\Sigma}^r$ has been obtained before and by using the Dyson's equation, the Green's function $\mathbf{G}^r$ is simply of the form

$$\mathbf{G}^r(\omega) = 1/(\omega\mathbf{I}_{2Nc} - \mathbf{H}_{\text{center}} - \mathbf{\Sigma}^r), \quad (17)$$

and in addition $\mathbf{G}^a = \mathbf{G}^{r\dagger}$, where $\mathbf{H}_{\text{center}}$ is the Hamiltonian of the center region in the Nambu representation.

In the numerical calculations, we take the hopping energy $t = t_c = 2.75$ eV and the nearest-neighbor carbon–carbon distance $a = 0.142$ nm as in a real graphene sample [3, 4].

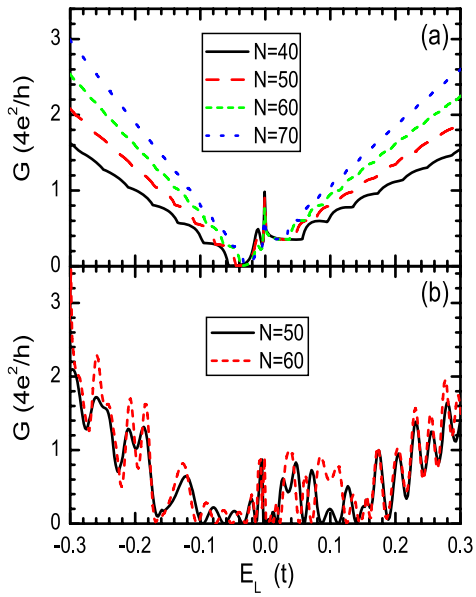

Figure 2. The linear conductance G versus the energy $E_{\rm L}$ for different width N at the clean system with $W = 0$. The panels (a) and (b) are for the magnetic field strength $\phi = 0$ and $\phi = 0.007$, respectively.

The superconductor gap Δ is set to $\Delta = t/2750 = 1$ meV and the Fermi wavevector $k_{\rm F} = 1$ Å^{-1}. The temperature $\mathcal{T}$ is set to zero since $\mathcal{T}$ can be as low as 1 K in a real experiment and thus $k_{\rm B}\mathcal{T}$ is much smaller than all other relevant energies, such as t and Δ. The magnetic field is expressed in terms of ϕ with $\phi \equiv (3\sqrt{3}/4)a^2B/\phi_0$ and $(3\sqrt{3}/2)a^2B$ is the magnetic flux in the honeycomb lattice. In the presence of disorder, the curves are averaged over up to 1000 random configurations.

3. The linear conductance

In this section, we consider the small bias limit and investigate the linear conductance. When the bias V is smaller than the gap Δ, the normal tunneling processes cannot occur and $T(\omega) = 0$ for $|\omega| < \Delta$. Then only Andreev reflection processes contribute to the current and the linear conductance $G = \lim_{V\to 0} {\rm d}I/{\rm d}V = (4e^2/h)T_{\rm A}(0)$ at zero temperature. In the following, we carry out numerical studies of graphene nanoribbons with both zigzag and armchair edges.

3.1. The zigzag edge case

First, we study the clean graphene nanoribbons with the disorder strength $W = 0$. Figure 2 shows the linear conductance G versus the on-site energy $E_{\rm L}$ (i.e. the energy at the Dirac point) with and without the magnetic field. The energy $E_{\rm L}$ can be controlled by the gate voltage in an experiment. For $E_{\rm L} > 0$, the charge carrier of graphene is hole-like, and it is electron-like for $E_{\rm L} < 0$. In the absence of a magnetic field ($\phi = 0$), the conductance G is approximately linear with $|E_{\rm L}|$ due to the linear increase of the carrier density. For a narrow graphene nanoribbon (e.g. $N = 40$), the conductance G clearly shows the step structures because of the sub-bands from the finite width. When a sub-band passes through the Fermi energy $E_{\rm F}$ ($E_{\rm F} = 0$), a step appears. For $N = 40$, the width of the graphene ribbon is $(3N - 1)a \approx 17$ nm. The graphene ribbon with this width has been realized in a recent experiment [21]. On the other hand, for a wide graphene nanoribbon (e.g. $N = 70$), the step structures fade away due to the reduction of the interval of the sub-bands.

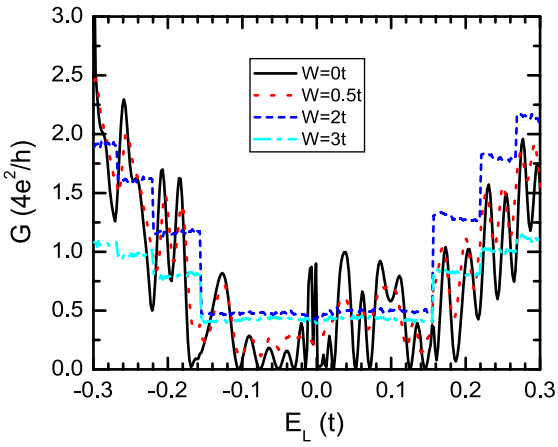

Figure 3. The conductance G versus $E_{\rm L}$ for the different disorder strengths W, with the parameters $L = 16$, $N = 60$ and $\phi = 0.007$.

While in the presence of a strong magnetic field, the conductance G does not show a clear pattern and depends strongly on $E_{\rm L}$ and the width N (see figure 2(b)). Raising the disorder from zero, the conductance G in the small-value region is increased while G in the large-value region is decreased (as shown in figure 3). Meanwhile some plateaus emerge at moderate disorder strength, e.g. $W = 2$.[3] These plateaus originate from the mixture of the electron and hole edge states, which will be discussed in detail in the last paragraph in this section.

Figure 4 shows the linear conductance G versus the on-site energy $E_{\rm L}$ with a moderate disorder strength W. G exhibits the plateaus with or without a magnetic field. In the absence of the magnetic field, the conductance G is similar to the disorder-free case (compare figures 2(a) and 4(a)) and the plateaus of the conductance are equal-spaced in energy. These plateaus are from the discrete sub-bands. In a graphene sample, due to the linear dispersion relation, the sub-bands are equal-spaced and so are the plateaus. For a wider graphene ribbon, the sub-bands are closer, then the widths of the plateaus are smaller, so that the plateaus are faded at large width (e.g. $N = 70$). On the other hand, in the presence of a magnetic field, the width of conductance plateaus are independent of the width N of the graphene ribbon, and the plateaus are always clear regardless of N. Now the plateaus are equal-spaced at the scale of $E_{\rm L}^2$ and the values of the conductance plateaus are determined by the filling factors ν of the Landau level and the width N of the graphene ribbon. The wider N is, the larger the

[3] In a recent paper [27], it shows that the Anderson localization occurs in the graphene systems and the conductance is very small at the disorder strength $W \sim t$. But in this work we only consider a graphene nanoribbon with small sizes, so the Anderson localization may not appear and the conductance can be large at the disorder strength $W \sim t$.

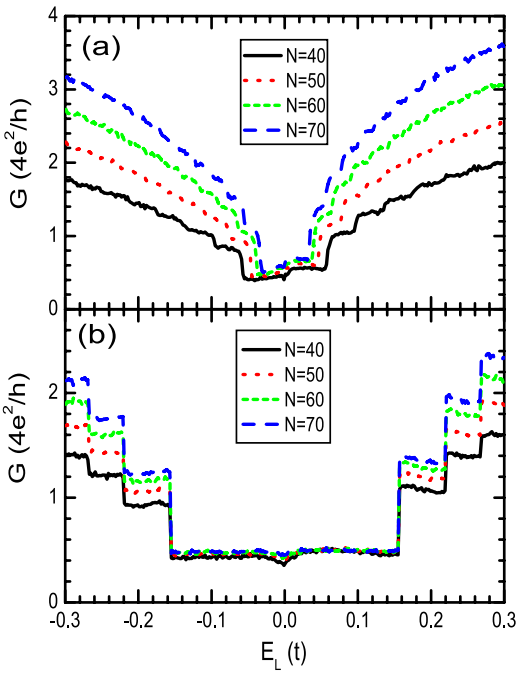

Figure 4. The conductance G versus the energy $E_{\rm L}$ for different width N at the moderate disorder strength $W = 2t$ and $L = 16$. Panels (a) and (b) are for the magnetic field strength $\phi = 0$ and $\phi = 0.007$, respectively.

conductance value is. But the conductance reaches a saturated value $|\nu|e^2/h$ at large N (see figure 5(b)). Figure 5 shows the conductance G versus the width N of the graphene ribbon. For $\phi = 0$, G increases approximately in a linear way with N (see figure 5(a)). But at high magnetic field G has a saturated value (see figure 5(b)). For a small filling factor (e.g. $E_{\rm L} = 0.1t$ with $\nu = 2$), G reaches the saturated value with small N ($N = 40$). For a large filling factor, G reaches the saturated value only with quite a large N.

With the aid of the edge states, these phenomena can be well explained. With a high magnetic field, the edge states that carry charges are formed. In the interface of the graphene and the superconductor, the edge states extend from one boundary to the other along the interface, in which the Andreev reflection occurs. So the wider the graphene ribbon is, the larger the probability is for the Andreev reflection. In the large N limit, the electron and hole edge states are well mixed. Thus, the Andreev reflection coefficient is 0.5, independent of any system parameters, such as the width N, the on-site energy $E_{\rm L}$, the magnetic field strength ϕ and the disorder strength W. Then the conductance $G = (2e^2/h)2T_{\rm A}(0) = |\mu|e^2/h$.

3.2. The armchair edge case

In this section, the linear conductance G in the armchair edge case is numerically investigated. Figure 6 shows the conductance G versus the on-site energy $E_{\rm L}$. Without a magnetic field ($\phi = 0$), G increases linearly with the energy $|E_{\rm L}|$ in the absence of disorder (see figure 6(a)). The disorder evidently enhances the conductance G in the small $|E_{\rm L}|$ region (see figure 6(b)). Thus G departs from the linear relation with $|E_{\rm L}|$. In contrast with the zigzag edge case, it has two obvious characteristics: (i) there is a zero conductance G region near $E_{\rm L} = 0$ for $N = 3m$ or $3m + 1$, because an energy gap emerges at the armchair edge graphene ribbon causing the Andreev reflection to vanish. This zero-conductance G region still exists in the presence of disorder (e.g. $W = 2$). (ii) The step structures from the sub-bands are not apparent, although the width of the graphene ribbon is $\sqrt{3}Na \approx 17$ nm for $N = 70$. For the zigzag edge case with this width the step structures are clearly seen (see figures 2(a) and 4(a)).

With a magnetic field, the Landau levels are formed and the conductance G departs completely from the linear relation with $|E_{\rm L}|$. For the clean system ($W = 0$), the conductance is quite small at the smallest filling factor $|\nu| = 2$ and exhibits some peaks at the higher filling factors $|\nu| = 6$, 10, 14, etc (see figure 6(c)). On the other hand, in the presence of disorder ($W = 2$), the conductance G shows plateaus and the plateau values are $|\nu|e^2/h$ in the large width N limit. This is because of the mixture of the electron and hole edge states and the Andreev reflection coefficient is 0.5 at large N. The characteristics of the plateaus at the moderate disorder strength are similar to that of the zigzag edge graphene ribbon.

Figure 7 shows the conductance G versus the width N of the graphene ribbon for a moderate disorder strength. At zero magnetic field, the conductance G increases linearly with the width N as it appears in a classical system. But at a high magnetic field, although the conductance G still increases with the width, a saturation value $|\nu|e^2/h$ appears, the same as in the zigzag edge case.

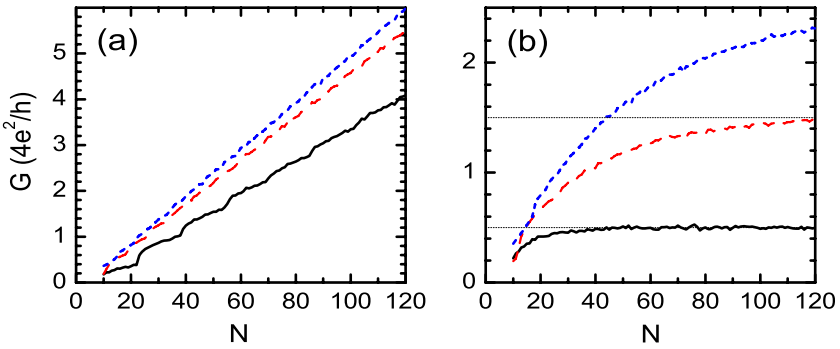

Figure 5. The conductance G versus the width N of the graphene nanoribbon with $E_{\rm L} = 0.1t$ (solid curve), $0.2t$ (dashed curve) and $0.25t$ (dotted curve). Panels (a) and (b) are for the magnetic field strengths $\phi = 0$ and $\phi = 0.007$, respectively. The other parameters are $W = 2$ and $L = 16$.

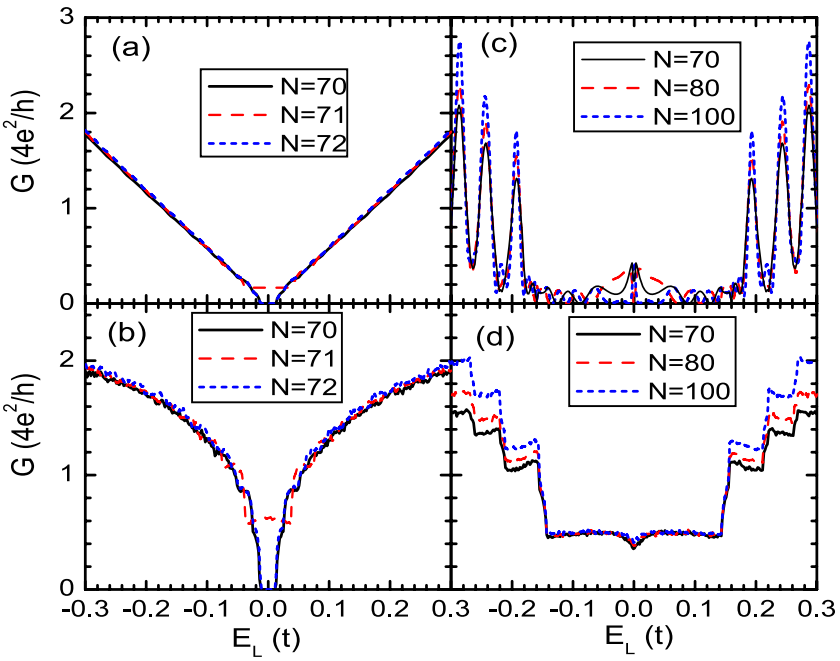

Figure 6. The conductance G versus the energy $E_{\rm L}$ for different widths N. The parameters are $L = 12$, the disorder strength $W = 0$ (in (a) and (c)) and $W = 2t$ (in (b) and (d)) and the magnetic field strength $\phi = 0$ (in (a) and (b)) and $\phi = 0.007$ (in (c) and (d)).

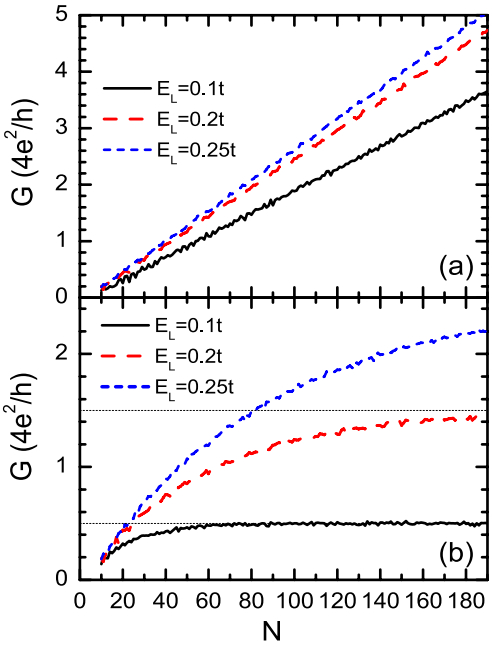

Figure 7. The conductance G versus the width N of the graphene nanoribbon for the different energies $E_{\rm L}$. Panels (a) and (b) are for the magnetic field strengths $\phi = 0$ and $\phi = 0.007$, respectively. The other parameters are $W = 2t$ and $L = 12$.

4. The finite bias case

In this section, the case with a finite bias is investigated. With the bias $V > \Delta$, the normal tunneling processes also occur and the current I is

$$I = \frac{2e}{h}\int {\rm d}\omega \{T(\omega)(f_\uparrow - f) + T_{\rm A}(\omega)(f_\uparrow - f_\downarrow)\}. \quad (18)$$

Following this, we numerically study the normal tunneling coefficient $T(\omega)$ and Andreev reflection coefficient $T_{\rm A}(\omega)$ for the zigzag edge graphene ribbon. Figure 8 shows $T(\omega)$ and $T_{\rm A}(\omega)$ versus the energy ω of the incident electron for the clean system. The normal tunneling coefficient $T(\omega)$ is zero when $|\omega| < \Delta$ because of the superconductor gap, and $T(\omega)$ is near 1 at $|\omega| > \Delta$ since there is no barrier at the interface of the superconductor and graphene. Next, we focus on the Andreev reflection coefficient $T_{\rm A}(\omega)$. For zero magnetic field with $\phi = 0$, $T_{\rm A}(\omega)$ is almost zero for $|\omega| > |E_{\rm L}|$ (see figure 8(a)), implying that the specular Andreev reflection is very weak at $\phi = 0$. But the usual Andreev retroreflection still occurs and $T_{\rm A}(\omega)$ is quite large for $|\omega| < |E_{\rm L}|$. With a magnetic field (see figure 8(c)), both kinds of Andreev reflections occur simultaneously and $T_{\rm A}(\omega)$ is always finite regardless of whether $|\omega| < |E_{\rm L}|$ or $|\omega| > |E_{\rm L}|$. $T_{\rm A}(\omega)$ has a peak at $\omega = \pm\Delta$ and quickly decays for $|\omega| > \Delta$, which is similar to a normal metal–superconductor junction [28].

Finally, the effect of the disorder on the normal tunneling coefficient $T(\omega)$ and Andreev reflection coefficient $T_{\rm A}(\omega)$ is studied. The normal tunneling coefficient $T(\omega)$ is almost unaffected by a moderate disorder strength W, $T(\omega)$ is still zero for $|\omega| < \Delta$ and near 1 for $|\omega| > \Delta$ (see figures 9(b) and (d)). However, the Andreev reflection coefficient $T_{\rm A}(\omega)$ is evidently affected by the disorder (see figures 9(a) and (c)). Both specular Andreev reflection and the usual Andreev retroreflection occur and $T_{\rm A}(\omega)$ is close to 0.5 in the whole range of $|\omega| < \Delta$.

5. Conclusion

In summary, by using the non-equilibrium Green's function method, the electron transport through the graphene nanoribbon–superconductor junction is investigated. Both

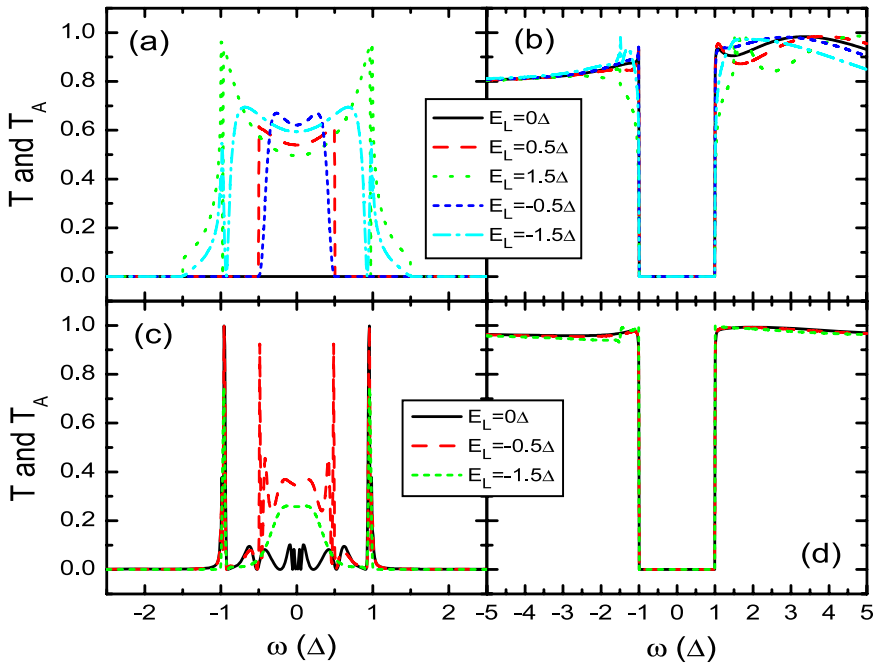

Figure 8. The normal tunneling coefficient $T(\omega)$ (in (b) and (d)) and Andreev reflection coefficient $T_A(\omega)$ (in (a) and (c)) versus ω for different on-site energy E_L. The other parameters are $N = 50$, $W = 0$ and the magnetic field strength $\phi = 0$ (in (a) and (b)) and $\phi = 0.007$ (in (c) and (d)).

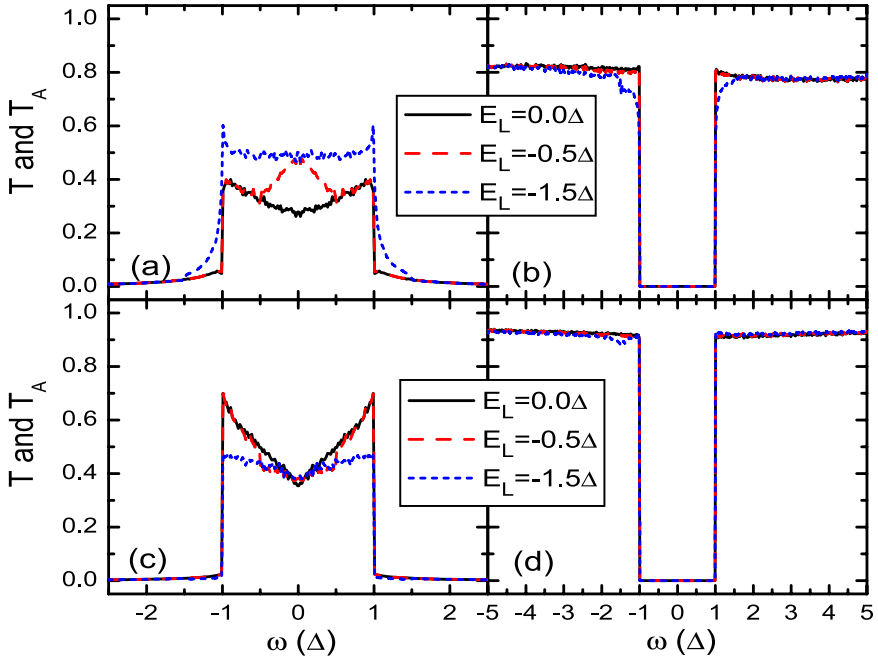

Figure 9. The normal tunneling coefficient $T(\omega)$ (in (b) and (d)) and Andreev reflection coefficient $T_A(\omega)$ (in (a) and (c)) versus ω for different on-site energy E_L. The other parameters are $N = 50$, $L = 16$, $W = 2t$ and the magnetic field strength $\phi = 0$ (in (a) and (b)) and $\phi = 0.007$ (in (c) and (d)).

zigzag and armchair edge graphene nanoribbons are considered. The effects of a magnetic field and disorder on the transport property are discussed. In the clean system and without a magnetic field, the linear conductance increases approximately in a linear fashion with the on-site energy for the case with the armchair edge or the wide zigzag edge. In the presence of a magnetic field and moderate disorder, the linear conductance exhibits the plateau structures for both armchair and zigzag edge nanoribbons. The plateau value increases with the width of the graphene ribbon, but reaches a saturation at $|\nu|e^2/h$ (ν is the filling factor) for the wide graphene ribbon. In addition, the case with a finite bias is studied and the dependence of the Andreev reflection and normal tunneling coefficients on the energy of the incident electron are discussed.

Acknowledgments

We gratefully acknowledge the financial support from NSF-China under grant nos. 10525418 and 10734110, and US-DOE under grant nos. DE-FG02-04ER46124 and US-NSF.

Appendix

In this appendix, we derive the surface Green's function $\mathbf{g}_{\mathrm{S}}^{r}$ of the superconductor lead and the self-energies $\mathbf{\Sigma}_{\mathrm{R}}^{r,a,<}$ of coupling to the superconductor lead. The definition of the surface Green's function $\mathbf{g}_{\mathrm{S}}^{r}$ is

$$\mathbf{g}_{\mathrm{S}}^{r}(y,y',t) = -\mathrm{i}\theta(t) \times \begin{pmatrix} \langle\{b_{\uparrow}(y,t), b_{\uparrow}^{\dagger}(y',0)\}\rangle & \langle\{b_{\uparrow}(y,t), b_{\downarrow}(y',0)\}\rangle \\ \langle\{b_{\downarrow}^{\dagger}(y,t), b_{\uparrow}^{\dagger}(y',0)\}\rangle & \langle\{b_{\downarrow}^{\dagger}(y,t), b_{\downarrow}(y',0)\}\rangle \end{pmatrix}$$

and $\mathbf{g}_{\mathrm{S}}^{r}(y,y',\omega)$ is the Fourier transformation of $\mathbf{g}_{\mathrm{S}}^{r}(y,y',t)$, where y and y' are the real-space positions on the surface of a half-infinite superconductor lead. Applying the equation of motion, $\mathbf{g}_{\mathrm{S}}^{r}(y,y',\omega)$ can be written as

$$\mathbf{g}_{\mathrm{S}}^{r}(y,y',\omega) = \sum_{\mathbf{k}} \frac{1}{\omega_{+}^{2} - \epsilon_{\mathbf{k}}^{2} - \Delta^{2}} \begin{pmatrix} \omega_{+} + \epsilon_{\mathbf{k}} & \Delta \\ \Delta & \omega_{+} - \epsilon_{\mathbf{k}} \end{pmatrix} \times \mathrm{e}^{\mathrm{i}k_{y}(y-y')},$$

where $\omega_{+} = \omega + \mathrm{i}0^{+}$. Next, we calculate the sum, $\sum_{\mathbf{k}} F(\mathbf{k})\mathrm{e}^{\mathrm{i}k_{y}(y-y')}$ with $F(\mathbf{k}) = (\omega_{+} \pm \epsilon_{\mathbf{k}})/(\omega_{+}^{2} - \epsilon_{k}^{2} - \Delta^{2})$ or $F(\mathbf{k}) = \Delta/(\omega_{+}^{2} - \epsilon_{k}^{2} - \Delta^{2})$:

$$\sum_{\mathbf{k}} F(\mathbf{k})\mathrm{e}^{\mathrm{i}k_{y}(y-y')} = \int_{-\pi}^{\pi} \mathrm{d}\theta \int \mathrm{d}k\, k\rho_{k}\mathrm{e}^{\mathrm{i}k(y-y')\sin\theta} F(k) = \int \mathrm{d}\epsilon_{k}\, J_{0}(k(y-y'))\rho(\epsilon_{k})F(k).$$

where J_0 is the Bessel function of the first kind, ρ_k is the density of state in the k space and $\rho(\epsilon_k) = 2\pi k\rho_k(\mathrm{d}k/\mathrm{d}\epsilon_k)$ is the density of state in the energy space. In the above steps, we have assumed the s-wave superconductor so that $\epsilon_{\mathbf{k}}$ only depends on $k = |\mathbf{k}|$. In the following, we assume that the density of state $\rho(\epsilon_k) = \rho$ is independent of the energy ϵ_k and $J_0(k(y-y'))$ only depends on the Fermi wavevector k_{F} [25]. These assumptions are reasonable because the main contribution to the transport behavior is these electrons with their energies near the Fermi energy. Then $\mathbf{g}_{\mathrm{S}}^{r}(y,y',\omega)$ reduces to

$$\mathbf{g}_{\mathrm{S}}^{r}(y,y',\omega) = J_{0}(k_{\mathrm{F}}(y-y'))\rho \times \int \mathrm{d}\epsilon_{k} \frac{1}{\omega_{+}^{2} - \epsilon_{k}^{2} - \Delta^{2}} \begin{pmatrix} \omega_{+} + \epsilon_{k} & \Delta \\ \Delta & \omega_{+} - \epsilon_{k} \end{pmatrix}.$$

By using the theorem of residue, the integration $\int \mathrm{d}\epsilon_k$ in the above equation can be obtained analytically [25], and the surface Green's function $\mathbf{g}_{\mathrm{S}}^{r}(y,y',\omega)$ changes into

$$\mathbf{g}_{\mathrm{S}}^{r}(y,y',\omega) = -\mathrm{i}\pi\rho J_{0}(k_{\mathrm{F}}(y-y'))\beta(\omega) \begin{pmatrix} 1 & \Delta/\omega \\ \Delta/\omega & 1 \end{pmatrix},$$

where $\beta(\omega) = |\omega|/\sqrt{\omega^{2} - \Delta^{2}}$ while $|\omega| > \Delta$ and $\beta(\omega) = \omega/(\mathrm{i}\sqrt{\Delta^{2} - \omega^{2}})$ while $|\omega| < \Delta$. After solving the surface Green's function $\mathbf{g}_{\mathrm{S}}^{r}(y,y',\omega)$, the self-energies $\mathbf{\Sigma}_{\mathrm{R}}^{r,a,<}$ are obtained straightforwardly:

$$\begin{aligned} \mathbf{\Sigma}_{\mathrm{R},ij}^{r}(\omega) &= t_{\mathrm{c}}\mathbf{g}_{\mathrm{S}}^{r}(y_i,y_j,\omega)t_{\mathrm{c}}^{*} \\ &= -\mathrm{i}\pi\rho|t_{\mathrm{c}}|^{2}J_{0}(k_{\mathrm{F}}(y_i-y_j))\beta(\omega) \begin{pmatrix} 1 & \Delta/\omega \\ \Delta/\omega & 1 \end{pmatrix} \\ &\equiv -(\mathrm{i}/2)\mathbf{\Gamma}_{\mathrm{R},ij}(\omega), \end{aligned}$$

$\mathbf{\Sigma}_{\mathrm{R}}^{a}(\omega) = (\mathrm{i}/2)\mathbf{\Gamma}_{\mathrm{R}}(\omega)$ and $\mathbf{\Sigma}_{\mathrm{R}}^{<}(\omega) = \mathrm{i}f(\omega)\mathbf{\Gamma}_{\mathrm{R}}(\omega)$.

References

[1] Novoselov K S, Geim A K, Morozov S V, Jiang D, Zhang Y, Dubonos S V, Grigorieva I V and Firsov A A 2004 *Science* **306** 666
Novoselov K S, Geim A K, Morozov S V, Jiang D, Katsnelson M I, Grigorieva I V, Dubonos S V and Firsov A A 2005 *Nature* **438** 197
[2] Zhang Y, Tan Y W, Stormer H L and Kim P 2005 *Nature* **438** 201
[3] Beenakker C W J 2008 *Rev. Mod. Phys.* **80** 1337
[4] Castro Neto A H, Guinea F, Peres N M R, Novselov K S and Geim A K 2009 *Rev. Mod. Phys.* **81** 109
[5] Beenakker C W J 2006 *Phys. Rev. Lett.* **97** 067007
[6] Akhmerov A R and Beenakker C W J 2007 *Phys. Rev.* B **75** 045426
Rainis D, Taddei F, Dolcini F, Polini M and Fazio R 2009 *Phys. Rev.* B **79** 115131
Greenbaum D, Das S, Schwiete G and Silvestrov P G 2007 *Phys. Rev.* B **75** 195437
[7] Linder J and Sudbø A 2007 *Phys. Rev. Lett.* **99** 147001
Linder J and Sudbø A 2008 *Phys. Rev.* B **77** 064507
[8] Titov M and Beenakker C W J 2006 *Phys. Rev.* B **74** 041401
Titov M, Ossipov A and Beenakker C W J 2007 *Phys. Rev.* B **75** 045417
[9] Moghaddam A G and Zareyan M 2006 *Phys. Rev.* B **74** 241403(R)
[10] Liang Q, Yu Y, Wang Q and Dong J 2008 *Phys. Rev. Lett.* **101** 187002
[11] Zhang Q, Fu D, Wang B, Zhang R and Xing D Y 2008 *Phys. Rev. Lett.* **101** 047005
Linder J, Yokoyamn T, Huertas-Hernando D and Sudbø A 2008 *Phys. Rev. Lett.* **100** 187004
Asano Y, Yoshida T, Tanaka Y and Golubov A A 2008 *Phys. Rev.* B **78** 014514
[12] Bhattacharjee S and Sengupta K 2006 *Phys. Rev. Lett.* **97** 217001
Bhattacharjee S, Maiti M and Sengupta K 2007 *Phys. Rev.* B **76** 184514
[13] Maiti M and Sengupta K 2007 *Phys. Rev.* B **76** 054513
[14] Burset P, Yeyati A L and Martin-Rodero A 2008 *Phys. Rev.* B **77** 205425
[15] Cuevas J C and Yeyati A L 2006 *Phys. Rev.* B **74** 180501(R)
[16] Zhang Z Y 2008 *J. Phys.: Condens. Matter* **20** 445220
Bai C, Yang Y and Zhang X 2008 *J. Phys.: Condens. Matter* **20** 335202
[17] Gonzalez J and Perfetto E X 2008 *J. Phys.: Condens. Matter* **20** 145218
[18] Andreev A F 1964 *Sov. Phys.—JETP* **19** 1228
[19] Heersche H B, Jarillo-Herrero P, Oostinga J B, Vandersypen L M K and Morpurgo A F 2007 *Nature* **446** 56
[20] Miao F, Wijeratne S, Zhang Y, Coskun U C, Bao W and Lau C N 2007 *Science* **317** 1530
[21] Li X, Wang X, Zhang L, Lee S and Dai H 2008 *Science* **319** 1229
[22] Sheng D N, Sheng L and Weng Z Y 2006 *Phys. Rev.* B **73** 233406
Qiao Z and Wang J 2007 *Nanotechnology* **18** 435402
[23] Long W, Sun Q F and Wang J 2008 *Phys. Rev. Lett.* **101** 166806

Li J and Shen S Q 2008 *Phys. Rev.* B **78** 205308
[24] Meir Y and Wingreen N S 1992 *Phys. Rev. Lett.* **68** 2512
Jauho A P, Wingreen N S and Meir Y 1994 *Phys. Rev.* B **50** 5528
[25] Sun Q F, Wang J and Lin T H 1999 *Phys. Rev.* B **59** 3831
Sun Q F, Wang J and Lin T H 1999 *Phys. Rev.* B **59** 13126
[26] Lee D H and Joannopoulos J D 1981 *Phys. Rev.* B **23** 4997
Lopez Sancho M P, Lopez Sancho J M and Rubio J 1984 *J. Phys. F: Met. Phys.* **14** 1205
Lopez Sancho M P, Lopez Sancho J M and Rubio J 1985 *J. Phys. F: Met. Phys.* **15** 851
[27] Aleiner I L and Efetov K B 2006 *Phys. Rev. Lett.* **97** 236801
[28] Blonder G E, Tinkham M and Klapwijk T M 1982 *Phys. Rev.* B **25** 4515